Higgs Searches at the Tevatron

Scott S. Snyder
Brookhaven National Laboratory, Upton, NY 11973, USA

This paper summarizes the current status of Higgs boson searches at the Fermilab Tevatron, as of summer 2004. Both Standard Model and non-Standard Model searches are discussed.

1. Introduction

One of the highest priority physics topics for the Fermilab Tevatron is the exploration of the Higgs sector of the Standard Model (SM). Previous searches at LEP have set a 95% C.L. lower limit for the mass of a Standard Model Higgs boson of $114.4\,\mathrm{GeV}/c^2$ [1]. Global fits of the Standard Model to all available electroweak data give a best-fit mass of $114\,\mathrm{GeV}/c^2$, with a 95% C.L. upper limit of $m_H < 260\,\mathrm{GeV}/c^2$ [2].

More discussion on the theory of the Higgs sector and on previous direct and indirect searches may be found in other papers from this School. Here, we concentrate on the features that are the most relevant for the analyses reported here. Additional background information about Higgs physics at the Tevatron and elsewhere may be found in [1, 3–6].

First, however, some terminology. The interaction cross section σ for high-energy physics processes is conventionally expressed in "barns," where $1\mathrm{b} = 10^{-24}\,\mathrm{cm}^2$. This is a large unit in this context; to set the scale, $\sigma(p\bar{p} \to W + X)$ is about 2 nb at the Tevatron, while $\sigma(p\bar{p} \to t\bar{t})$ is about 7 pb. The observed event rate for a process is proportional the cross section; the proportionality constant is called the *luminosity* $\mathcal{L}$, conventionally measured in units of $\mathrm{cm}^{-2}\,\mathrm{s}^{-1}$. Finally, the amount of data accumulated by an experiment over a period of time is quantified by the *integrated luminosity*, $\int \mathcal{L}\,dt$. This is typically stated in units of pb^{-1} or fb^{-1}. The total number of events of a given kind expected is then the process cross section times the integrated luminosity.

The production cross sections for Higgs bosons at the Tevatron for several different processes are shown in Figure 1, while the decay branching ratios are shown in Figure 2. There are, broadly speaking, two mass ranges of interest. For low Higgs boson masses, $m_H \lesssim 140\,\mathrm{GeV}/c^2$, the dominant decay is $H \to b\bar{b}$. The dominant production mechanism is $gg \to H$; however, it is clear that $gg \to H \to b\bar{b}$ is completely hopeless in the face of the large background of $b\bar{b}$ production from other sources. So, in this mass range, one needs to look for the associated production of a Higgs boson along with a W or Z boson, which can then decay leptonically. At higher Higgs boson masses, the decay $H \to WW$ dominates. For this process, the backgrounds are sufficiently under control that one can search for $gg \to H \to WW$ directly. For either process, the production cross section is ~ 0.1–1 pb.

There are some other possible channels. $Ht\bar{t}$ would have a spectacular final state signature, but with a total production cross section of ~ 5 fb, this is a very difficult channel for the Tevatron. $Hb\bar{b}$ has a similarly small cross section; however, some extensions to the Standard Model predict enhancements to this mode. Decays involving $H \to \gamma\gamma$ are likewise not feasible at the Tevatron with the Standard Model branching ratios, but some alternative models predict enhancements.

This paper is structured as follows. Section 2 summarizes relevant features of the Tevatron collider and the two detectors. Sections 3 and 4 describe the various Higgs boson search analyses which have been conducted, in both Standard Model and non-Standard Model scenarios, respectively. Section 5 discusses prospects for future Higgs boson searches at the Tevatron, and Section 6 contains the conclusions.

2. The Tevatron and the detectors

Until the LHC turns on, the Fermilab Tevatron is the only instrument in the world capable of probing the Higgs sector of the Standard Model. Located near Chicago, it collides protons against antiprotons in a ring of supercon-

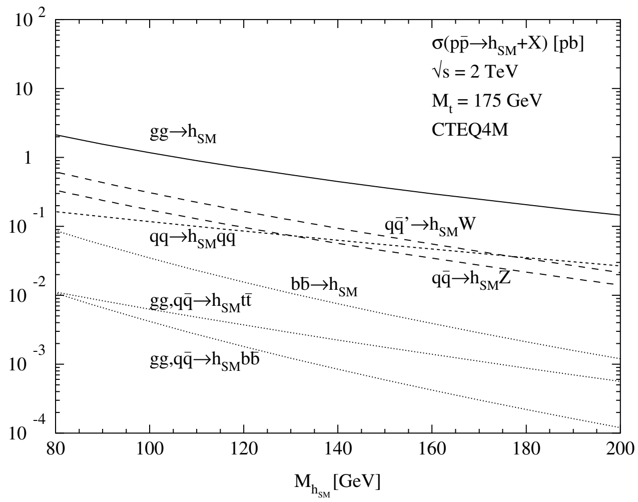

Figure 1: Higgs boson production cross sections at the Tevatron, as a function of Higgs boson mass [3, 7].

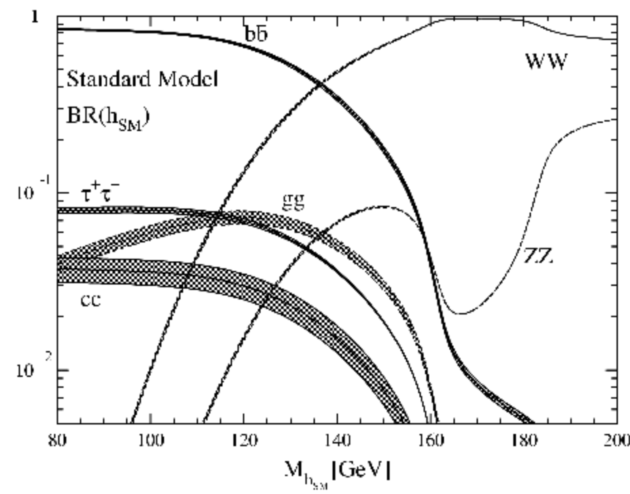

Figure 2: Higgs boson decay branching ratios, as a function of Higgs boson mass [3, 7, 8].

ducting magnets about 6 km in circumference. During the last run of the collider, from 1992 to 1996 ("Run I"), the Tevatron had a center-of-mass collision energy of 1.8 TeV, and a time between collisions of 3.5 μs. For the current run ("Run II"), the energy has been raised to 1.96 TeV, and the collision spacing has been shortened to 396 ns.

A schematic of the accelerator complex is shown in Figure 3. The proton beam originates with a Cockroft-Walton pre-accelerator, is raised to 400 MeV in a linear accelerator, and then boosted to 8 GeV in the booster, a fast-cycling synchrotron about 150 m in diameter. From there, beam is transferred to the larger Main Injector and accelerated to 120–150 GeV. From there, beam can be transferred to the Tevatron, where it will be accelerated to the full 980 GeV beam energy. But beam from the Main Injector can also be used to make antiprotons. First, beam from the Main Injector is directed onto a metal target. Antiprotons are selected from the products of this reaction and stored in the antiproton Accumulator, where they are "cooled" to reduce their momentum spread. From the Accumulator, the antiprotons can be fed back into the Main Injector and then to the Tevatron in order to use them for collisions. One other storage ring in the complex is called the Recycler; it operates at 8 GeV and is constructed mainly from permanent magnets. The original idea of the Recycler was to be able to recover the antiprotons remaining in the Tevatron after a store was completed, re-cool them, and use them again in another store. This mode of operation has yet to be implemented. Recently, however, the Recycler has been used as a place to store antiprotons in addition to the Accumulator (the rate at which antiprotons can be added to the Accumulator goes down as it fills up). Antiprotons can then be transferred to the Main Injector from both the Accumulator and Recycler. The result of such "mixed mode" operations has been the highest Tevatron luminosities to date.

Although the collider run got off to somewhat of a slow start, within the last year the collider has exceeded even the optimistic goals that had been set for that year. Peak luminosities have exceeded $100 \times 10^{30}/\,\mathrm{cm}^2/\,\mathrm{s}$, and about $350\,\mathrm{pb}^{-1}$ were delivered in 2004, making a total of over $600\,\mathrm{pb}^{-1}$ for the run so far.

There are two large, general-purpose experiments at the Tevatron, CDF [9] and DØ [10]. The layouts of these two detectors are sketched in Figure 4. Though different in detail, they share the same general features. Starting from the inside, they contain at the center a tracking system, which can measure in three dimensions the trajectories of charged particles going through it. This is placed within a solenoidal magnetic field, in order to allow a measurement of the particles' momenta. The innermost portion of the tracking system uses very precise silicon detectors, in order to allow tagging tracks which are displaced slightly from the collision point due to the decay of a long-lived particle. Surrounding the tracking system is the calorimeter, which consists of an absorber material, sufficient to stop most particles going through it, interleaved with devices to measure the amount of energy deposited. This allows a measurement of the total energy of a particle (or narrow cluster of particles) and its direction. The calorimeter stops most particles with the exception of muons and neutrinos. Muons are detected with another set of tracking

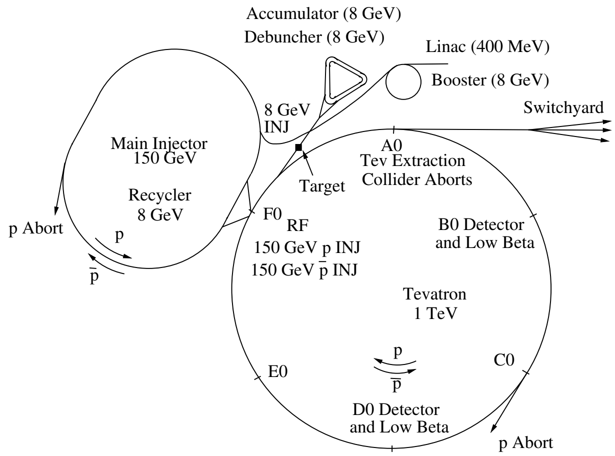

Figure 3: Schematic of the Fermilab accelerator complex (not to scale).

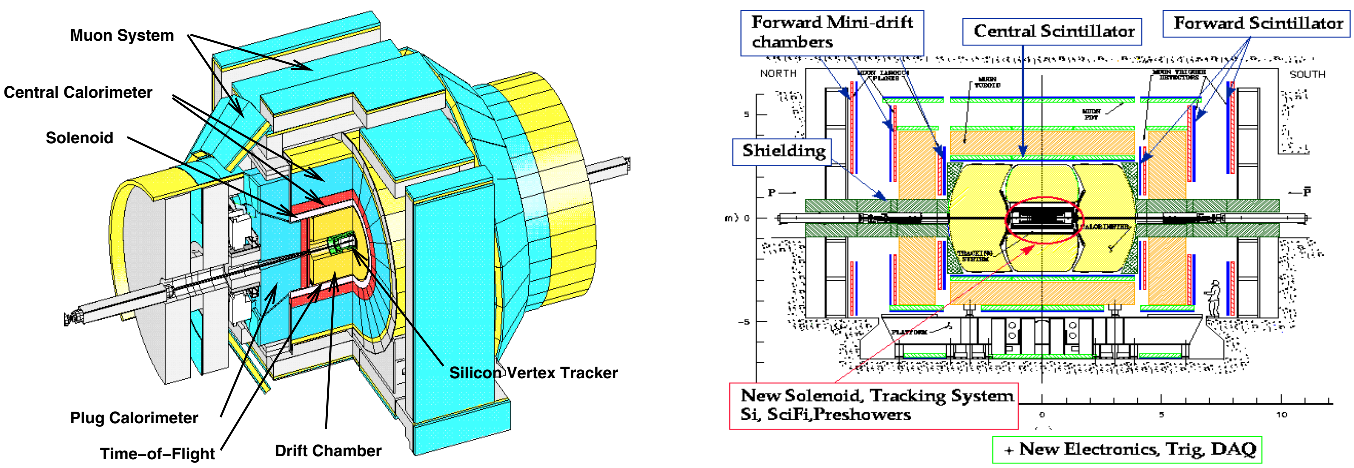

Figure 4: Diagrams of the CDF (left) and DØ (right) detectors..

chambers that surround the calorimeter.

At hadron colliders, it is convenient to use a cylindrical coordinate system. The center-of-mass frame of the collision has an unknown boost along the direction of the beam (it cannot be measured well since a significant amount of energy leaves the collision at very small angles to the beam and escapes down the beam pipe). So, rather than talk about the energy or momentum of a particle, it is more usual to refer only to the vector component perpendicular to the beam axis. This is called “transverse” energy or momentum, denoted as E_T or p_T. It is also conventional to express the polar angle as the “psuedorapidity” $\eta \equiv -\ln\tan\theta/2$.

The detectors are designed to be very good at identifying electrons and muons. An electron is identified by looking for a deposit of energy in the inner (“electromagnetic”) portion of the calorimeter, along with a matching charged particle track. (Electrons and photons deposit most of their energy much nearer the inner part of the calorimeter than do hadronic particles.) Typically, requirements are also made on the shape of the deposit. Muons are identified by looking for tracks in the muon chambers outside the calorimeter. Often, a matching track in the central part of the detector is also required, possibly along with a small deposit of energy in the calorimeter consistent with the passage of a muon. For the analyses being discussed here, the electrons and muons are usually required to be “isolated” — that is, there are no other large deposits of energy in the calorimeter nearby.

A quark or gluon will appear in the final state as a “jet” of particles in a narrow cone. Jets are detected as clusters of energy in the calorimeter. Because many of the processes of interest for Higgs boson physics have b-jets in the final state, it is essential to be able to distinguish such jets from jets formed from light quarks or gluons (this is called

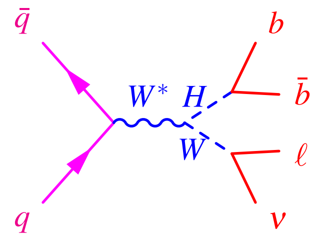

Figure 5: Feynman diagram for the $WH \to \ell\nu b\bar{b}$ process.

"b-tagging"). There are two general ways in which this is done. First, some fraction of the time, a b-jet will contain a muon, through either $b \to \mu$ or $b \to c \to \mu$. One can thus identify a b-jet by looking for a muon embedded in a jet. Such muons, however, are usually of rather low p_T, and can be difficult to identify efficiently. (One can, in principle, also use electrons in addition to muons; however, it is much more difficult to identify an electron embedded in a jet than a muon.) The second method takes advantage of the fact that B mesons have a relatively long lifetime, and can travel a macroscopic distance ($\sim 1\,\mathrm{mm}$) from the collision point before decaying The innermost tracking systems of both experiments are designed to be able to measure track trajectories with the precision necessary to do this. This second method is significantly more effective than the first; the analyses reported here use this method exclusively.

The presence of a neutrino is inferred by looking for an imbalance in the total transverse energy in the event. This imbalance, or "missing E_T," is written as "$\not\!\!E_T$".

3. Standard Model Higgs boson searches

3.1. $WH \to \ell\nu b\bar{b}$

This channel, where a H boson is produced in association with a W boson, with $H \to b\bar{b}$ and $W \to \ell\nu$ (see Figure 5), is the most powerful single channel for Higgs at the Tevatron. The final state consists of one high-p_T lepton, large $\not\!\!E_T$, and two b-jets. The backgrounds can be divided into two classes, "physics" and "instrumental." Physics backgrounds are those that actually have the same final state as the process for which we're searching, for example $Wb\bar{b}$ with $W \to \ell\nu$. Instrumental backgrounds are those in which the final state is actually different from the one for which we're searching, but it appears to be the same. For example, instrumental backgrounds to this channel would include $p\bar{p} \to Wjj$ (where j denotes a light quark jet) where a light quark jet is misidentified as a b-jet, heavy flavor production $p\bar{p} \to b\bar{b}j\ldots$ where a jet is misidentified as a lepton and the $\not\!\!E_T$ is substantially mismeasured, and light quark production $p\bar{p} \to jjj\ldots$ where all the above occur. These backgrounds are kept under control by imposing tight requirements on the leptons, b-jets, and $\not\!\!E_T$ in order to obtain good purity.

Among the physics backgrounds, the largest is $Wb\bar{b}$ production. This background can be suppressed somewhat by imposing requirements on the momenta and relative angles of the final state objects, but the main handle for reducing this background is by requiring that the $b\bar{b}$ invariant mass be close to the assumed mass of the Higgs boson. The second largest background is $t\bar{t}$ production, with either $t\bar{t} \to b\bar{b}jj\ell\nu$ or $t\bar{t} \to b\bar{b}\ell\nu\ell'\nu$. The $t\bar{t}$ background can be reduced by vetoing on the presence of extra jets or leptons in the event. Other physics backgrounds that must be considered include single top production $p\bar{p} \to t\bar{b}$ and vector boson pair production $p\bar{p} \to WZ$.

Both experiments have carried out analyses in this channel. The DØ analysis [11] uses electrons only, and is based on a sample with $\int \mathcal{L}\,dt = 174\,\mathrm{pb}^{-1}$. They require exactly one isolated electron with $E_T > 20\,\mathrm{GeV}$, $\not\!\!E_T > 25\,\mathrm{GeV}$, and exactly two jets with $E_T > 20\,\mathrm{GeV}$ and $|\eta| < 2.5$. Next, both jets are required to be b-tagged. The $m(b\bar{b})$ distributions that result after requiring 0, 1, and 2 b-tags are shown in Figure 6. A total of 6 events pass this selection, compared to 4.44 ± 1.17 expected from Standard Model processes, including 1.72 ± 0.41 from $Wb\bar{b}$ (see Table I). The dominant systematic uncertainties on the acceptances are due to b-tagging efficiency (11%) and jet energy corrections (7% for $Wb\bar{b}$). Including uncertainties on the Monte Carlo (MC) cross sections (18%) and luminosity (6.5%) gives a total

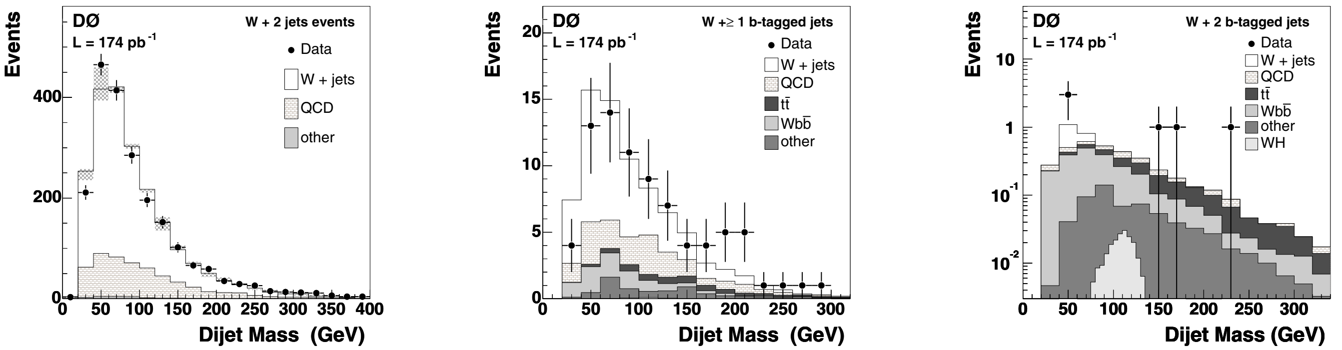

Figure 6: $m(b\bar{b})$ distribution in the DØ WH analysis after requiring 0, 1, and 2 b-tags. [11]

Table I: Summary table for DØ WH analysis, comparing observed event counts to the Standard Model expectations. The WH expectation is for $m_H = 115\,\mathrm{GeV}/c^2$. The last column, with three or more jets, is not used in this analysis, but is included as a check of the background estimate. [11]

	$W+\geq 2$ jets	$W+2$ jets	$W+$ 2 jets (1 b-tagged jet)	$W+2$ jets (2 b-tagged jets)	$W+\geq 3$ jets (2 b-tagged jets)
WH	0.6 ± 0.1	0.4 ± 0.1	0.14 ± 0.03	0.056 ±0.013	0.015 ±0.004
WZ	1.4 ± 0.3	1.2 ± 0.3	0.38 ± 0.09	0.13 ± 0.03	0.02 ± 0.01
$Wb\bar{b}$	24.7 ± 6.2	21.4 ± 5.3	6.6 ± 1.5	1.72 ± 0.41	0.37 ± 0.09
$t\bar{t}$	41.4 ± 8.7	8.6 ± 1.8	2.7 ± 0.6	0.78 ± 0.19	4.63 ± 1.11
Single-top	11.6 ± 2.4	8.3 ± 1.7	2.7 ± 0.6	0.47 ± 0.11	0.30 ± 0.07
QCD multijet	492 ± 108	393 ± 86	17.1 ± 4.3	0.50 ± 0.20	0.92 ± 0.37
W or Z+jets	2008 ± 502	1672 ± 418	43.0 ± 12.9	0.78 ± 0.22	0.86 ± 0.24
Total expectation	2580 ± 626	2106 ± 513	72.6 ± 20.0	4.44 ± 1.17	7.12 ± 1.89
Observed events	2540	2116	76	6	7

systematic uncertainty on the Standard Model expectation of 26%. The total efficiency for $Wb\bar{b}$ is $(0.90 \pm 0.14)\%$, which allows setting an an upper limit on the $Wb\bar{b}$ production cross section of

$$\sigma(Wb\bar{b}) < 6.6\,\mathrm{pb} \text{ at 95\% C.L., for } p_T(b) > 20\,\mathrm{GeV}/c \text{ and } \Delta R(b\bar{b}) > 0.75.\ [(\Delta R)^2 = (\Delta\eta)^2 + (\Delta\phi)^2]$$

In order to set a limit on WH production, the dijet invariant mass $m(b\bar{b})$ is required to be within the window 85–135 GeV/c^2 (for $m_H = 115\,\mathrm{GeV}/c^2$). This leaves no observed events, with an expected background of 1.07 ± 0.26 and an expected WH signal of 0.049 ± 0.012. The signal efficiency is $(0.21 \pm 0.03\%)$. With no observed signal, this yields the limit

$$\sigma(WH) \times B(H \to b\bar{b}) < 9.0\,\mathrm{pb} \text{ at 95\% C.L. for } m_H = 115\,\mathrm{GeV}/c^2.$$

The same procedure was carried out for $m_H = 105$, 125, and 135 GeV/c^2. In the corresponding mass windows, 0, 0, and 1 events were observed. The results are plotted in Figure 7.

The CDF analysis of this channel [12], using 162 pb^{-1} of data, has a few major differences. Most importantly, CDF requires only one b-tag instead of two. Also, CDF uses both electrons and muons, rather than only electrons. CDF's initial event selection requires one isolated electron or muon with $E_T > 20\,\mathrm{GeV}$, no other leptons, $\not\!\!E_T > 20\,\mathrm{GeV}$, and exactly two jets with $E_T > 15\,\mathrm{GeV}$ and $|\eta| < 2$, one of which is tagged. Some additional requirements are also made to reject events with additional soft jet activity and events with extra isolated, high-p_T charged tracks. This selection yields 62 events, with an expected Standard Model background of 66.5 ± 9.0 events. A summary of the event counts is in Table II, and the systematic uncertainties are summarized in Table III.

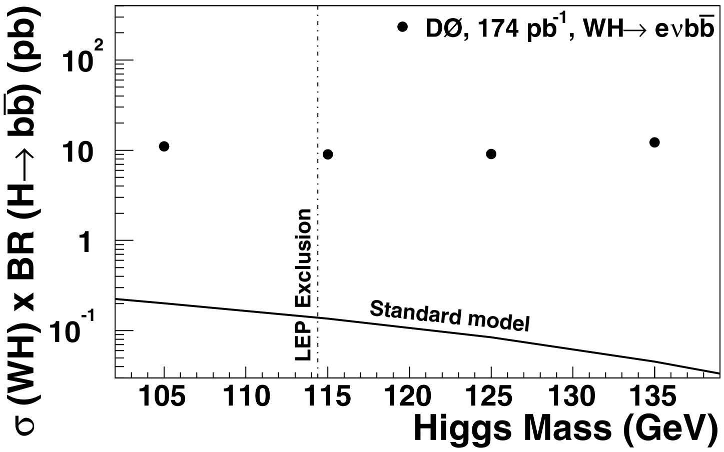

Figure 7: 95% C.L. upper limits on $\sigma(p\bar{p} \to WH) \times B(H \to b\bar{b})$ for the DØ WH analysis, compared to the Standard Model expectation. [11]

Table II: Summary table for the CDF WH analysis, comparing observed event counts to the Standard Model expectations. [12]

	$W+$jet	$W+$2jets	$W+$3jets	$W+\geq$ 4jets
Events before tagging	13417	2072	313	82
Mistags	36.2 ± 7.1	14.1 ± 2.6	4.0 ± 0.9	2.0 ± 0.5
$Wb\bar{b}$	32.2 ± 10.2	19.1 ± 5.8	3.7 ± 1.1	0.7 ± 0.2
$Wc\bar{c}$	11.9 ± 3.5	6.8 ± 2.2	1.2 ± 0.4	0.2 ± 0.1
Wc	30.0 ± 8.0	6.5 ± 1.8	1.0 ± 0.3	0.1 ± 0.0
Diboson/$Z \to \tau\tau$	1.7 ± 0.6	2.5 ± 0.6	0.5 ± 0.1	0.1 ± 0.0
non-W	20.3 ± 2.0	8.5 ± 1.2	2.8 ± 0.5	1.1 ± 0.2
$t\bar{t}$	0.4 ± 0.1	5.1 ± 1.0	12.8 ± 2.4	20.3 ± 3.7
single top	1.2 ± 0.2	3.8 ± 0.5	0.9 ± 0.1	0.2 ± 0.0
Total Background	133.9 ± 17.5	66.5 ± 9.0	26.9 ± 3.2	24.8 ± 3.8
Observed tags	135	62	23	21

Table III: Systematic uncertainties for the CDF WH analysis. [12]

Lepton ID	5%
Trigger efficiency	$< 1\%$
Parton distribution function	2%
Initial-state radiation	3%
Final-state radiation	6%
Jet energy scale	3%
b-tagging efficiency	6%
Jet energy resolution	1%
Total	11%

The dijet mass peak that results after this event selection is shown in Figure 8. No significant excess of the observed signal over the background is seen, so CDF proceeds to set a limit. The acceptance for WH as a function of Higgs boson mass varies approximately linearly from $(1.5 \pm 0.2)\%$ at $m_H = 110\,\mathrm{GeV}/c^2$ to $(1.7 \pm 0.2)\%$ at $m_H = 150\,\mathrm{GeV}/c^2$. This is converted to a cross section limit in Figure 9, giving the following result:

$$\sigma(WH) \times B(H \to b\bar{b}) < 5\,\mathrm{pb} \text{ at 95\% C.L. for } m_H = 115\,\mathrm{GeV}/c^2.$$

3.2. $ZH \to \ell\ell b\bar{b}$

This is the companion channel to WH, with a Z boson replacing the W boson. The dominant physics background here is $Zb\bar{b}$, and the product of cross section and branching ratio for both the signal and the dominant background are down by about a factor of 6 from the WH case. This makes this channel quite difficult at the Tevatron. At this point, the only analysis related to this channel that has been reported is a measurement by DØ of the ratio $\sigma(Z+b)/\sigma(Z+j)$, using both $Z \to ee$ and $Z \to \mu\mu$ decays [13]. The analysis uses about $180\,\mathrm{pb}^{-1}$ of data. Besides the presence of a Z boson decay, the analysis requires at least one jet with $E_T > 20\,\mathrm{GeV}$ and $|\eta| < 2.5$. Counting the number of events with and without b-tags then leads to the result (taking the $\sigma(Z+c)/\sigma(Z+b)$ ratio from theory):

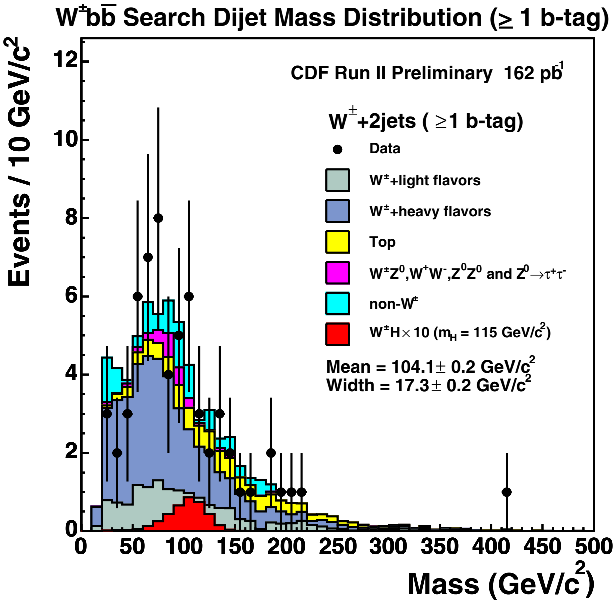

Figure 8: $m(b\bar{b})$ distribution in the CDF WH analysis after all selection requirements. [12]

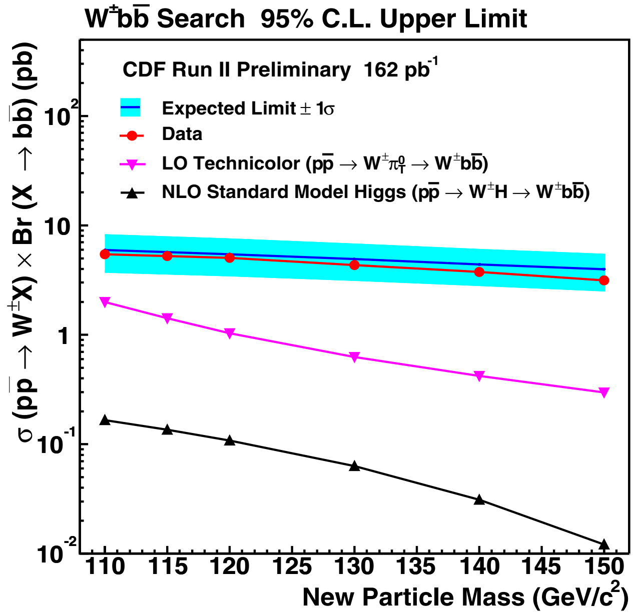

Figure 9: The 95% C.L. upper limit for the WH production cross section (times branching ratio) as a function of Higgs boson mass, for the CDF WH analysis. [12]

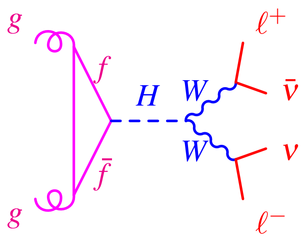

Figure 10: Feynman diagram for the $gg \to H \to WW^* \to \ell\ell\nu\nu$ process.

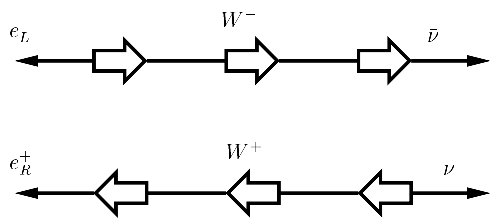

Figure 11: The leptons tend to go in the same direction due to the correlation of the W boson spins.

$$\sigma(Z+b)/\sigma(Z+j) = 0.023 \pm 0.004(\text{stat.})^{+0.002}_{-0.003}(\text{syst.}),$$

which is in good agreement with the theoretical NLO expectation of 0.018 ± 0.004 [14].

3.3. $H \to WW^* \to \ell\ell\nu\nu$

The other Standard Model Higgs process that is relevant at the Tevatron is $H \to WW^* \to \ell\ell\nu\nu$ (see Figure 10). This mode is significant for higher Higgs boson masses, $m_H \gtrsim 140\,\text{GeV}/c^2$. The final state signature consists of two isolated, opposite-sign leptons, large $\not{E}_T$, and small jet activity. Another characteristic of the signal that can be exploited is the fact that the spins of the W bosons from H boson decay are correlated (see Figure 11); consequently, the two leptons tend to go in the same direction. This implies small $m(\ell\ell)$ and small $\Delta\phi(\ell\ell)$. The backgrounds to this process include electroweak WW production, $Z/\gamma \to \ell\ell$ with mismeasured $\not{E}_T$, $W+$jets with a jet misidentified as a lepton, and WZ and ZZ.

Both experiments have reported results for this channel. Both use all three lepton combinations, ee, $e\mu$, and $\mu\mu$, except that the DØ analysis keeps the three channels separate until the end, while the CDF analysis combines them from the start.

The selection requirements used in the DØ analysis [15] are summarized in Table IV. The selection follows that

Table IV: Summary of signal selection requirements for the DØ $H \to WW^* \to \ell\ell$ analysis. The quantity $\not\!\!E_T^{\rm scaled} = \not\!\!E_T/[\sqrt{E_T(j)}\sin\theta(j)|\cos\Delta\phi(j,\not\!\!E_T)|]$ is used to reject events where $\not\!\!E_T$ is generated due to a mismeasurement of jet energy. $M_T^{\rm min}$ is the smaller of the transverse masses formed by the $\not\!\!E_T$ and either the electron or muon; this rejects $Z/\gamma* \to \tau\tau$ decays. (The transverse mass of two objects 1 and 2 is $M_{T12} = \sqrt{2p_{T1}p_{T2}[1-\cos(\phi_1-\phi_2)]}$). [15]

	ee: $\int \mathcal{L}\,dt = 177 \pm 12\,\mathrm{pb}^{-1}$	$e\mu$: $\int \mathcal{L}\,dt = 158 \pm 10\,\mathrm{pb}^{-1}$	$\mu\mu$: $\int \mathcal{L}\,dt = 147 \pm 10\,\mathrm{pb}^{-1}$
sel 1	$E_T(e_1) > 12$ GeV, $E_T(e_2) > 8$ GeV Opposite charge	$E_T(e) > 12$ GeV, $p_T(\mu) > 8$ GeV/c Opposite charge	$p_T(\mu_1) > 20$ GeV/c, $p_T(\mu_2) > 10$ GeV/c Opposite charge $m(\mu\mu) > 20$ GeV/c^2
sel 2	$\not\!\!E_T > 20$ GeV	$\not\!\!E_T > 20$ GeV	$\not\!\!E_T > 30$ GeV and $\not\!\!E_T > 0.75p_T(\mu_1) + 10$ GeV
sel 3	$12\,\mathrm{GeV}/c^2 < m(ee) < 80\,\mathrm{GeV}/c^2$	$M_T^{\rm min} > 20\,\mathrm{GeV}/c^2$	$\lvert m(\mu\mu) - M_Z\rvert > 15\,\mathrm{GeV}/c^2$
sel 4	$E_T(e_1) + E_T(e_2) + \not\!\!E_T > 100$ GeV	$E_T(e) + p_T(\mu) + \not\!\!E_T > 90$ GeV	—
sel 5	$\Delta\phi(ee) < 1.5$	$\Delta\phi(e\mu) < 2.0$	$\Delta\phi(\mu\mu) < 2.0$
sel 6	$\not\!\!E_T^{\rm scaled} > 15\sqrt{\mathrm{GeV}}$	$\not\!\!E_T^{\rm scaled} > 15\sqrt{\mathrm{GeV}}$	—
sel 7	No jets or 1 jet with $E_T(j_1) < 90$ GeV or $E_T(j_1) < 50$ GeV and $E_T(j_2) < 30$ GeV	No jets or 1 jet with $E_T(j_1) < 90$ GeV or $E_T(j_1) < 50$ GeV and $E_T(j_2) < 30$ GeV	No jets or $E_T(j_1) < 60$ GeV and $E_T(j_2) < 30$ GeV

Table V: Event counts for the DØ $H \to WW^* \to \ell\ell$ analysis, after the lepton preselection and after all selections. [15]

	ee		$e\mu$		$\mu\mu$	
	sel 1	sels 1–7	sel 1	sels 1–7	sel 1	sels 1–7
$t\bar{t} \to \ell_1\ell_2 bb\nu\nu$	3.05 ± 0.05	0.06 ± 0.01	3.98 ± 0.08	0.13 ± 0.01	3.15 ± 0.03	0.03 ± 0.003
$WZ \to \ell_1\ell_2 + X$	1.48 ± 0.03	0.04 ± 0.01	0.34 ± 0.01	0.11 ± 0.01		
$\Upsilon \to ee$	280.1 ± 6.2	0.0 ± 0.01				
W + jets	18.3 ± 0.3	1.24 ± 0.07	7.2 ± 0.1	0.34 ± 0.02		
$WW \to \ell_1\ell_2\nu\nu$	6.84 ± 0.06	1.17 ± 0.02	10.28 ± 0.09	2.51 ± 0.05	4.64 ± 0.05	1.28 ± 0.03
$Z/\gamma* \to \tau\tau$	133.6 ± 4.4	0.0 ± 0.1	168.5 ± 4.7	0.0 ± 0.1	57.7 ± 2.2	0.0 ± 0.0
$Z/\gamma* \to ee$	15895 ± 47	0.1 ± 0.1				
$Z/\gamma* \to \mu\mu$			5.2 ± 0.8	0.0 ± 0.05	8426 ± 27	3.9 ± 0.6
QCD	972 ± 31	0.0 ± 0.5	25.2 ± 2.4	0.0 ± 0.2		
QCD/W + jets					5.4 ± 0.6	0.02 ± 0.02
Total	17311 ± 57	2.7 ± 0.4	220.8 ± 5.3	3.1 ± 0.3	8497 ± 27	5.3 ± 0.6
Observed	17274	2	218	2	8509	5

outlined above: two energetic leptons, large $\not\!\!E_T$, and small jet activity. In addition, DØ requires $\Delta(\ell\ell) < 1.5$ in the ee channel, and < 2.0 in the $e\mu$ and $\mu\mu$ channels. The results of these selections are tabulated in Table V and are plotted in Figure 12 and Figure 13.

To extract a cross section limit, the signal efficiencies are also evaluated. These, together with the 95% C.L. cross section limits are given in Table VI. The limit as a function of m_H is also plotted in Figure 14. The result for $m_H = 160\,\mathrm{GeV}/c^2$ is

$$\sigma(gg \to H) \times B(H \to WW) < 5.7\,\mathrm{pb}.$$

CDF has also reported an analysis for this channel [17], using $184 \pm 11\,\mathrm{pb}^{-1}$ of data. As mentioned earlier, CDF combines the three channels together from the beginning. CDF also selects events using $m(\ell\ell)$, but they do not put

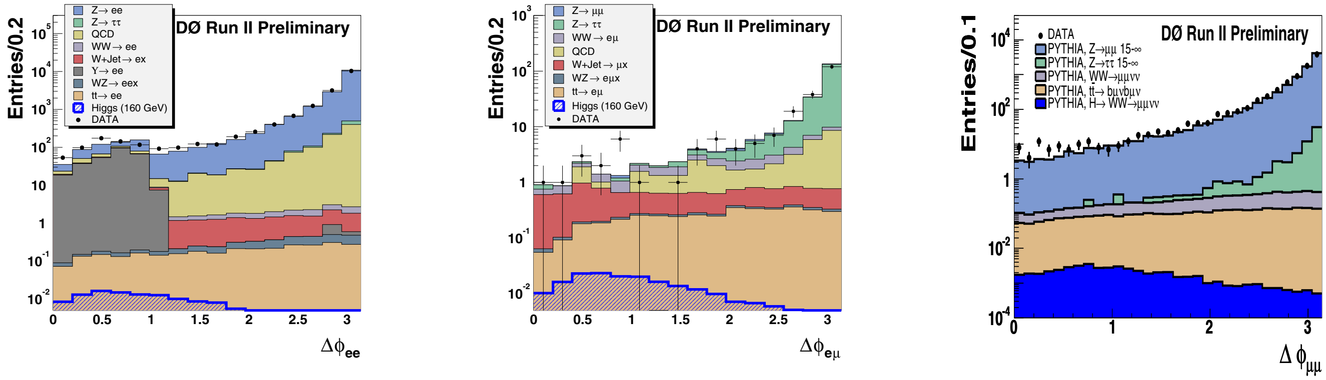

Figure 12: $\Delta\phi(\ell\ell)$ distributions in the DØ $H \to WW^* \to \ell\ell$ analysis, after the first selection has been applied. [15]

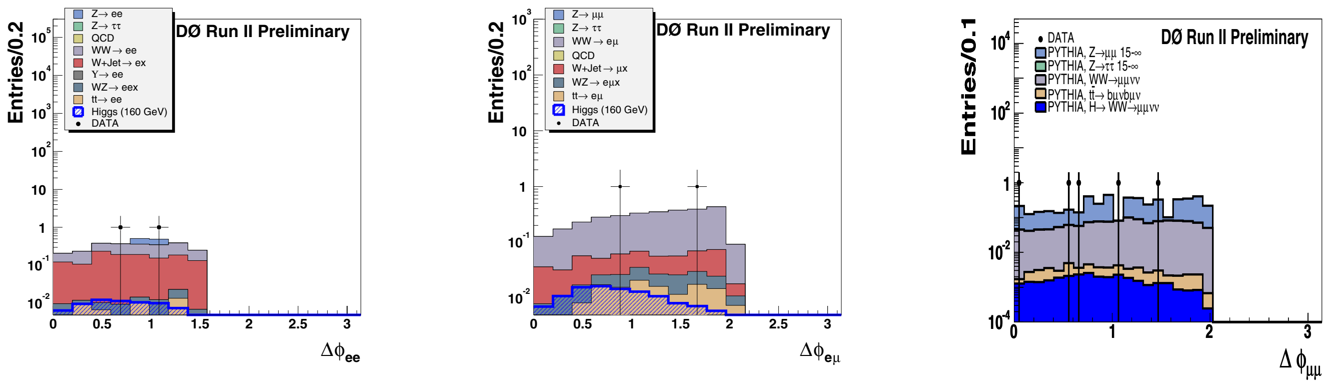

Figure 13: $\Delta\phi(\ell\ell)$ distributions in the DØ $H \to WW^* \to \ell\ell$ analysis, after the all selections have been applied. [15]

a requirement on $\Delta\phi(\ell\ell)$, instead fitting the entire distribution.

CDF uses the following requirements to select events for this analysis:

- Exactly two isolated, opposite-sign leptons (electron or muon) with $E_T > 20\,\text{GeV}$.
- $\not\!\!E_T > 25\,\text{GeV}$.
- No jets with $E_T > 15\,\text{GeV}$ and $|\eta| < 2.5$.
- $\not\!\!E_T > 50\,\text{GeV}$ or $\Delta\phi(\not\!\!E_T, o) > 20°$, where o is the closest lepton or jet.

Table VI: Signal efficiency and 95% C.L. $\sigma \times B$ limits for the DØ $H \to WW^* \to \ell\ell$ analysis. [15]

m_H (GeV/c^2)	100	120	140	160	180	200
Signal efficiency						
ee	0.023 ± 0.002	0.077 ± 0.003	0.104 ± 0.003	0.155 ± 0.004	0.151 ± 0.004	0.118 ± 0.003
$e\mu$	0.014 ± 0.001	0.059 ± 0.002	0.094 ± 0.003	0.131 ± 0.004	0.137 ± 0.004	0.130 ± 0.004
$\mu\mu$	0.045 ± 0.002	0.110 ± 0.003	0.150 ± 0.004	0.216 ± 0.005	0.179 ± 0.005	0.151 ± 0.004
$\sigma \times B(H \to WW)$ limit						
ee	102.2	29.7	21.8	14.8	15.2	19.2
$e\mu$	90.0	21.0	13.1	9.6	9.2	9.6
$\mu\mu$	86.4	35.2	25.8	17.9	21.6	25.7
All	40.1	12.0	8.2	5.7	5.8	6.6

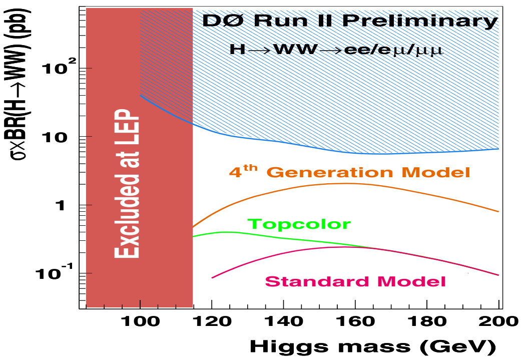

Figure 14: Excluded cross section times branching ratio $\sigma(gg \to H) \times B(H \to WW^*)$ at 95% C.L. together with expectations from Standard Model Higgs boson production and alternative models. The LEP limit on the standard model Higgs boson production is taken from [1], the fourth generation model is presented in [16], and the topcolor model is presented in [3]. For the DØ $H \to WW^* \to \ell\ell$ analysis. [15]

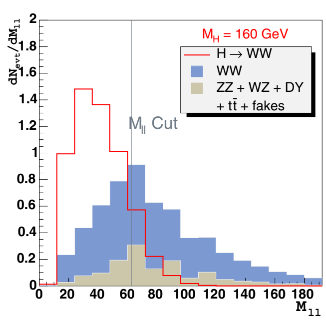

Figure 15: The $m(\ell\ell)$ distributions for the signal ($m_H = 160\,\mathrm{GeV}/c^2$), the $WW \to \ell\nu\ell\nu$ background, and the sum of other SM backgrounds (predicted by MC), normalized to expectations for $184\,\mathrm{pb}^{-1}$. (CDF $H \to WW^* \to \ell\ell$ analysis. [17])

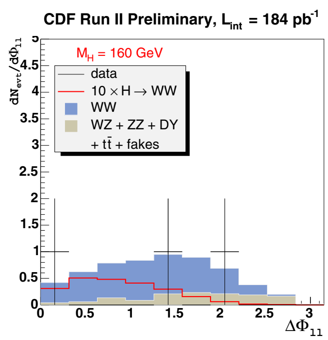

Figure 16: The $\Delta\phi(\ell\ell)$ distribution for the $m_H = 160\,\mathrm{GeV}/c^2$ case of the CDF $H \to WW^* \to \ell\ell$ analysis. Also shown are the results of fitting the signal and background distributions. [17]

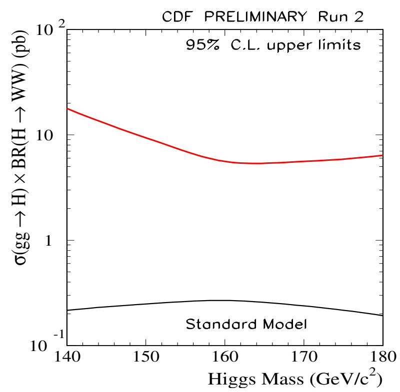

Figure 17: The 95% C.L. upper limits for $\sigma(gg \to H) \times B(H \to WW)$ for the CDF $H \to WW^* \to \ell\ell$ analysis, compared with Standard Model expectations. [17]

- If the leptons have identical flavor, $m(\ell\ell)$ must be outside the range 76–106 GeV, unless $\not{E}_T/\sigma(\not{E}_T) > 3$.
- A requirement is also made on $m(\ell\ell)$, depending on m_H (see Table VIII). This is useful for removing the dominant Standard Model backgrounds; see Figure 15.

The expected backgrounds for this analysis are listed in Table VII. To obtain the Higgs boson production cross section limit, CDF plots the $\Delta(\ell\ell)$ distributions and fits them to a sum of the expected signal and background. This distribution for $m_H = 160\,\mathrm{GeV}/c^2$ is shown in Figure 16. The results for all analyzed Higgs boson masses are summarized in Table VIII, and the resulting cross section limits are plotted in Figure 17. The result for $m_H = 160\,\mathrm{GeV}/c^2$ is

$$\sigma(gg \to H) \times B(H \to WW) < 5.6\,\mathrm{pb}.$$

Table VII: Summary of background expectations for the $m_H = 180\,\text{GeV}/c^2$ case for the CDF $H \to WW^* \to \ell\ell$ analysis. [17]

Source	WW	WZ	ZZ	DY ee	DY $\mu\mu$	DY $\tau\tau$	$t\bar{t}$	fakes
Expectation	6.49 ± 0.76	0.18 ± 0.02	0.06 ± 0.01	0.87 ± 0.44	0.43 ± 0.19	0.03 ± 0.01	0.02 ± 0.01	0.81 ± 0.25
Source	Total bkg	$H \to WW$ signal	Data					
Expectation	8.90 ± 0.98	0.17 ± 0.02	8					

Table VIII: Summary of results for the CDF $H \to WW^* \to \ell\ell$ analysis. [17]

Higgs mass (GeV/c^2)	140	150	160	170	180
$\sigma(gg \to H)$ (pb)	0.45	0.36	0.30	0.25	0.21
$B(H \to WW)$	0.48	0.68	0.90	0.97	0.94
$m(\ell\ell) <$	$55.0\,\text{GeV}/c^2$	$57.5\,\text{GeV}/c^2$	$62.5\,\text{GeV}/c^2$	$70.0\,\text{GeV}/c^2$	$80.0\,\text{GeV}/c^2$
Total acceptance (%)	0.124 ± 0.012	0.228 ± 0.023	0.402 ± 0.040	0.476 ± 0.048	0.449 ± 0.045
Expected signal (events)	0.10 ± 0.01	0.15 ± 0.02	0.22 ± 0.03	0.22 ± 0.03	0.17 ± 0.02
WW background (events)	3.51 ± 0.41	3.82 ± 0.45	4.45 ± 0.52	5.38 ± 0.63	6.49 ± 0.76
Other background (events)	0.68 ± 0.16	0.90 ± 0.24	1.34 ± 0.35	1.91 ± 0.47	2.40 ± 0.55
Candidate data (events)	2	2	3	7	8
95% C.L. limit — counting (pb)	18.4	9.8	6.2	8.2	8.8
Expected limit — $\Delta\phi$ fit (pb)	18.1	9.8	6.0	7.4	8.0
95% C.L. limit — $\Delta\phi$ fit (pb)	17.8	9.4	5.6	5.6	6.4

4. Non-Standard Model Higgs boson searches

4.1. Higgs boson decays to γ pairs

In addition to the decays discussed previously, Higgs bosons can decay into pairs of photons. This is a particularly clean signature, and would be very promising in a hadron collider environment. In fact, it is one of the decay modes favored for a Higgs boson discovery at the LHC. However, in the Standard Model, the branching ratio $B(H \to \gamma\gamma)$ is on the order of 10^{-3}–10^{-4}, which is too small for this channel to be feasible at the Tevatron [18]. But, many extensions to the Standard Model predict that the coupling of Higgs bosons to fermions is suppressed [19–27]. For example, in so-called "fermiophobic" models, the Higgs boson does not couple to any fermions, while in "topcolor" models, the only fermion to which the Higgs boson couples is the top quark. With the fermionic decay modes suppressed, the $H \to \gamma\gamma$ decay is enhanced. There are wide variety of such models, which make different quantitative predictions. According to [18], it is important to be prepared for any diphoton branching fraction, even up to 100%. Figure 18 shows calculations of the diphoton branching ratio for several different models.

The DØ experiment has carried out a search for this decay mode, using $191 \pm 13\,\text{pb}^{-1}$ of data [28]. Photon candidates are selected by looking for isolated clusters in the EM calorimeter with no matching track in the central detector. (Further requirements are made on the cluster shape.) The analysis requires two photon candidates with $E_T > 25\,\text{GeV}$. There is also a requirement on the transverse momentum of the diphoton system: $p_T(\gamma\gamma) > 35\,\text{GeV}/c$. Events are classified based on the location of the photon candidates:

- CCCC: Both candidates are in the central calorimeter.
- CCEC: One candidate is in the central calorimeter and one is in an end calorimeter.
- ECEC: Both candidates are in an end calorimeter.

The major backgrounds in this channel include direct diphotons, which is estimated from Monte Carlo, Drell-Yan $Z/\gamma^* \to ee$ in which the electrons are misidentified as photons, and QCD events in which one or more jets are

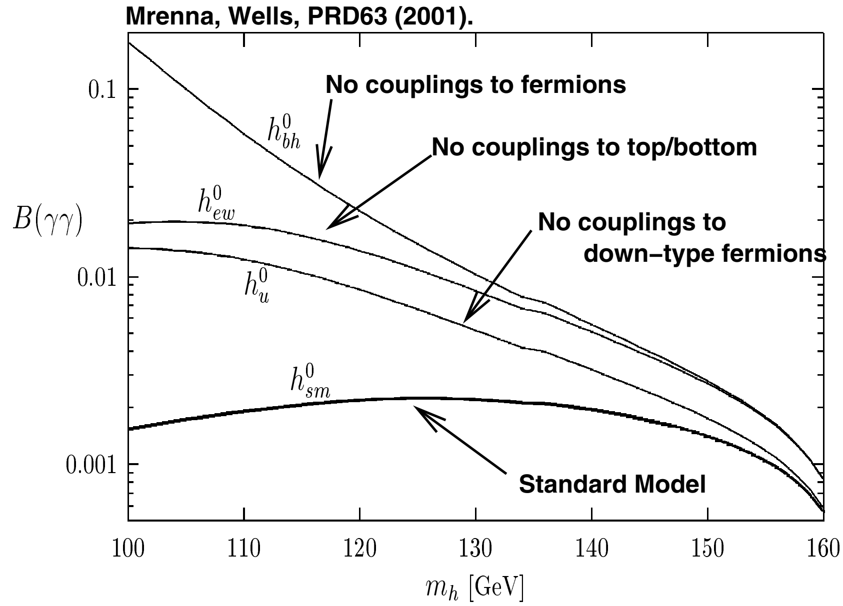

Figure 18: Branching ratio $B(H \to \gamma\gamma)$ as a function of m_H for several different models. [18].

misidentified as photons. The latter two backgrounds are estimated from data. The results of the selection and the background estimates are shown in Figure 19.

For the branching ratio limit extraction, only the CCCC and CCEC events are used. Two scenarios are considered: fermiophobic and topcolor models. For each scenario, Higgs boson masses between 60 and 150 GeV/c^2 are considered. A final selection is made on the diphoton invariant mass $m(\gamma\gamma)$ in a window around the Higgs boson mass. The width of this window depends on the scenario and on the Higgs boson mass, varying from about $6\,\mathrm{GeV}/c^2$ at $m_H = 60\,\mathrm{GeV}/c^2$ to about $10\,\mathrm{GeV}/c^2$ at $m_H = 150\,\mathrm{GeV}/c^2$. The efficiency for the mass window requirement is about 80%; the efficiency for the other requirements varies from about 1% to 30%, depending on Higgs boson mass and scenario. The extracted limits are plotted in Figure 20.

4.2. Supersymmetric Higgs bosons

In the framework of the Minimal Supersymmetric Standard Model (MSSM), there are five physical Higgs bosons [3]: two CP-even neutral scalars, h and H, one CP-odd neutral scalar, A, and two charged scalars, $H^\pm$. The Higgs sector of the theory can then be described by two parameters [4, pp. 10-28], which can be taken to be the mass of one of the scalars and $\tan\beta$, which is defined as the ratio of the vacuum expectation values of the two Higgs doublets. In general, the couplings of the neutral scalars ($\phi \equiv h/H/A$) to down-type quarks (such as b) are enhanced by a factor of $\tan\beta$. The cross section for producing a Higgs boson along with b-jets then goes as $\tan^2\beta$. Thus, for large $\tan\beta$, it is worthwhile to look for the process $p\bar{p} \to \phi b\bar{b}$, with $\phi \to b\bar{b}$. The diagrams for this process are shown in Figure 21, and Figure 22 shows the result of a leading-order calculation of the production cross section for two different values of $\tan\beta$.

In previous work, LEP has excluded at 95% C.L. a ϕ with $m_\phi < 91\,\mathrm{GeV}/c^2$ for all values of $\tan\beta$ [33]. In Run I, CDF excluded at 95% C.L. values of $\tan\beta > 60$–100 for m_ϕ in the range 91–200 GeV/c^2 [34].

In Run II, DØ has searched for a Higgs boson in the processes $p\bar{p} \to \phi b$ and $p\bar{p} \to \phi b\bar{b}$ with $\phi \to b\bar{b}$ using $131\,\mathrm{pb}^{-1}$ of data [35]. They select events with at least three b-tagged jets, and no more than four jets in total, then look for a peak in the dijet invariant mass distribution. The exact requirements used vary with the Higgs boson mass, see Table IX. The major background here is QCD multijet production, both with light jets and with b and c jets. This

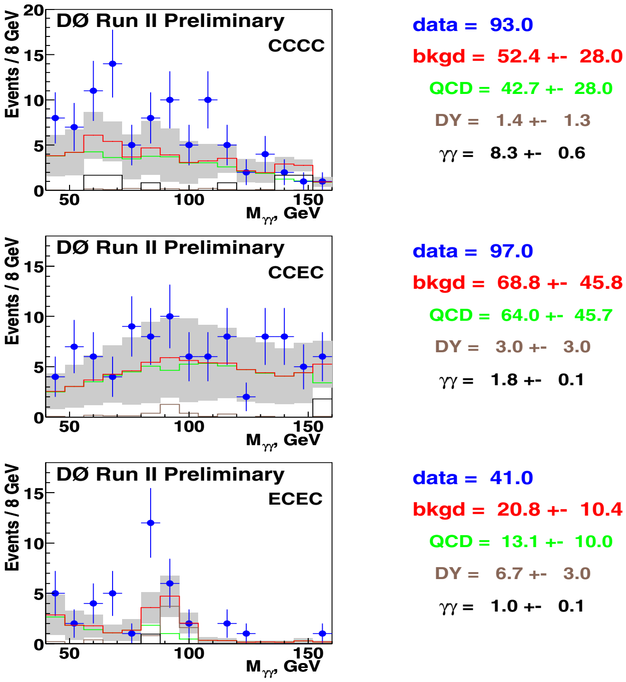

Figure 19: Diphoton invariant mass distributions and event yields for the DØ $H \to \gamma\gamma$ analysis. Shown are the measured data points and the expected Standard Model background. The gray band shows the uncertainty of the Standard Model estimate. [28]

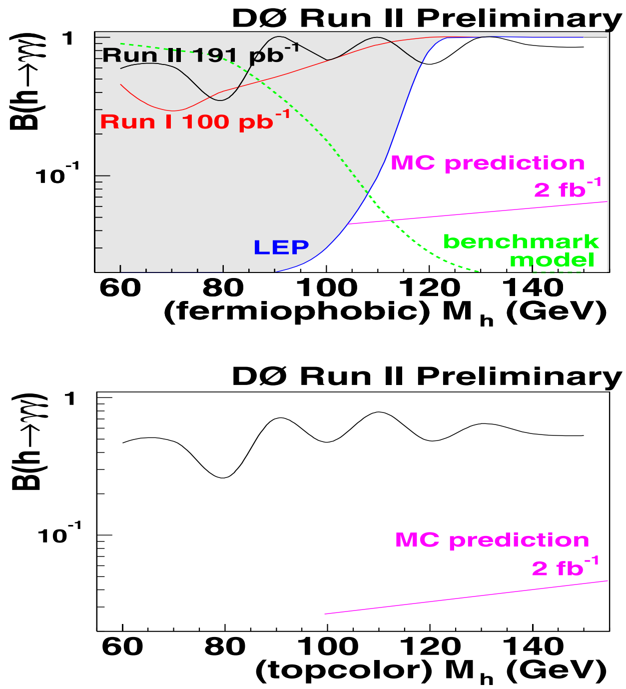

Figure 20: 95% C.L. limits on $B(H \to \gamma\gamma)$ for the DØ $H \to \gamma\gamma$ analysis, plotted separately for the fermiophobic and topcolor scenarios. The lower line shows the prediction for the limit that could be set during the current Tevatron run with $2\,\text{fb}^{-1}$ of data [29]. The top plot also shows exclusion results from DØ Run I [30] and LEP [31], and also a theoretical prediction for one possible model [32]. [28]

Figure 21: Feynman diagrams for $p\bar{p} \to \phi b\bar{b}$ production.

is evaluated using data. There are also smaller backgrounds from $(Z \to b\bar{b})j$ and $t\bar{t}$ processes, which are evaluated using Monte Carlo. The next step is to plot the distribution of the invariant masses of the two leading jets. This distribution is shown for $m_\phi = 120\,\text{GeV}/c^2$ in Figure 23. The distribution is then fit to a sum of signal and background to derive the limit in the $\tan\beta$—m_ϕ plane. The next-to-leading-order calculation of [36] is used for this. The result is plotted in Figure 24.

4.3. Doubly-charged Higgs bosons

Some models predict the existence of doubly-charged Higgs bosons [20, 37–46]. For example, left-right symmetric models [39–44] require a Higgs triplet, containing doubly-charged Higgs bosons. These models assume that parity is a good symmetry at high energies, but that it is spontaneously broken at lower energies. Other Higgs triplet models [20, 37, 45] as well as Little-Higgs models [46] also predict doubly-charged scalars. As long as the decays

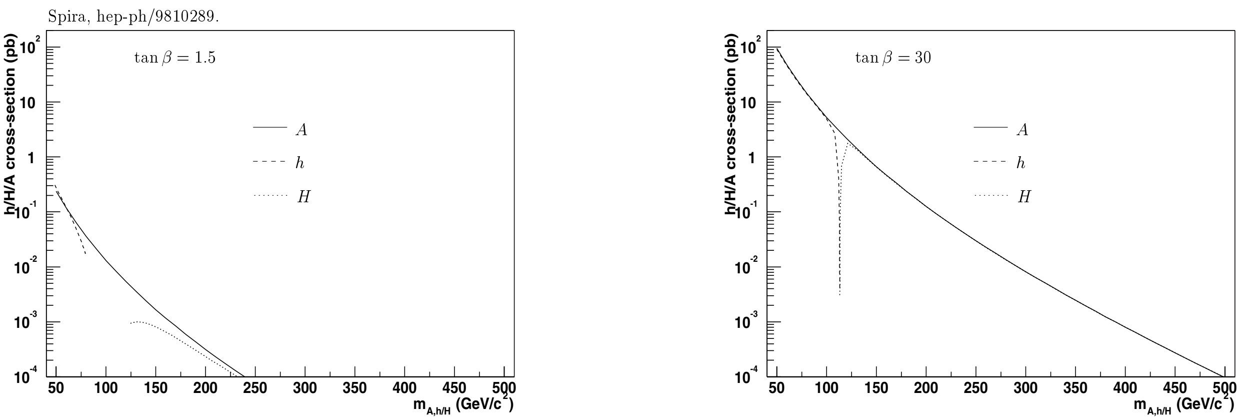

Figure 22: Production cross sections for neutral Higgs bosons along with a $b\bar{b}$ pair at leading order for $\tan\beta = 1.5$ (left) and 30 (right). [7]

Table IX: Event selection requirements, signal acceptances, and systematic uncertainties for the DØ $\phi b\bar{b}$ analysis. [35]

	Event selection requirements				Acceptance (%)				Syst. uncertainty (%)	
m_H (GeV/c^2)	$E_T(j_1)$	$E_T(j_2)$	$E_T(j_3)$	$\lvert\eta\rvert$	Kinematic	Trigger	b-tag	Total	Acceptance	Background
100	> 45 GeV	> 35 GeV	> 15 GeV	< 2.5	4.75	59	17	0.48	22.4	10.0
120	> 45 GeV	> 35 GeV	> 15 GeV	< 2.5	8.55	62	17	0.89	22.5	9.8
150	> 60 GeV	> 40 GeV	> 15 GeV	< 2.0	13.2	71	16	1.5	21.8	9.6

$H^{\pm\pm} \to H^\pm H^\pm$ and $H^{\pm\pm} \to H^\pm W^\pm$ are kinematically disallowed, the dominant decay mode is expected to be into same-sign charged leptons. These decays violate lepton number conservation, so decays with two different lepton flavors are also possible. The branching ratios are not well constrained, but some constraints on the lepton couplings have been set using data from LEP and $g-2$ [47–49]. LEP experiments have also set mass limits on $H^{\pm\pm}$, assuming exclusive decays to one lepton flavor, of about $m(H^{\pm\pm}) > 100\,\text{GeV}/c^2$ [50–52].

The coupling of $H^{\pm\pm}$ to $W^\pm W^\pm$ is experimentally constrained to be small [53]. Therefore, the dominant production

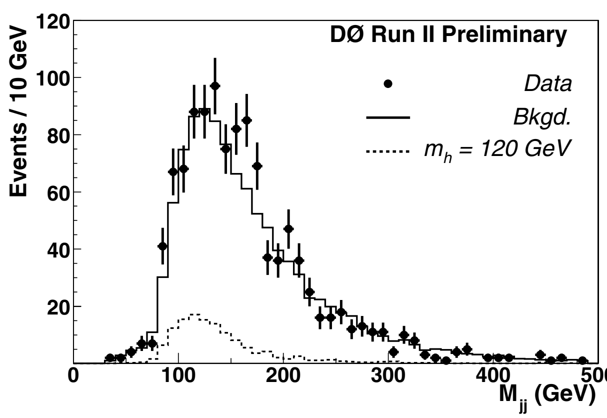

Figure 23: The distribution of the invariant mass of the leading two jets from the triple b-tagged data of the DØ $\phi b\bar{b}$ analysis. Also plotted are the estimated background and the Higgs boson signal at the 95% C.L. exclusion limit. This is for the $m_\phi = 120\,\text{GeV}/c^2$ case. [35]

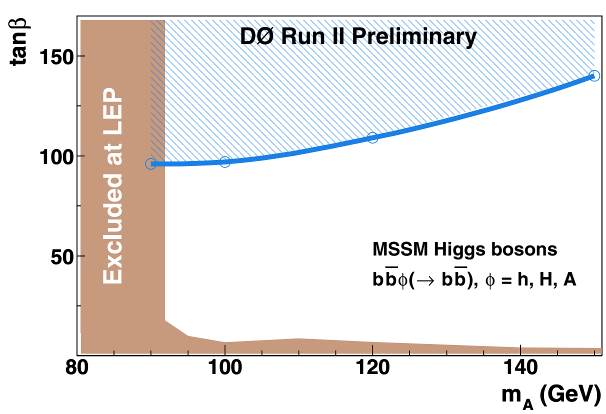

Figure 24: The 95% C.L. lower limit on $\tan\beta$ as a function of m_ϕ for the DØ $\phi b\bar{b}$ analysis. [35]

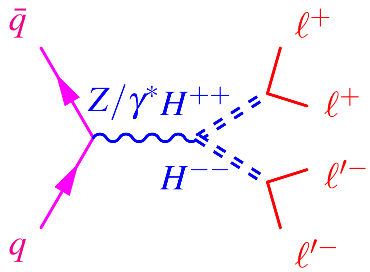

Figure 25: Feynman diagram for the $q\bar{q} \to H^{++}H^{--} \to \ell^+\ell^+\ell^-\ell^-$ process.

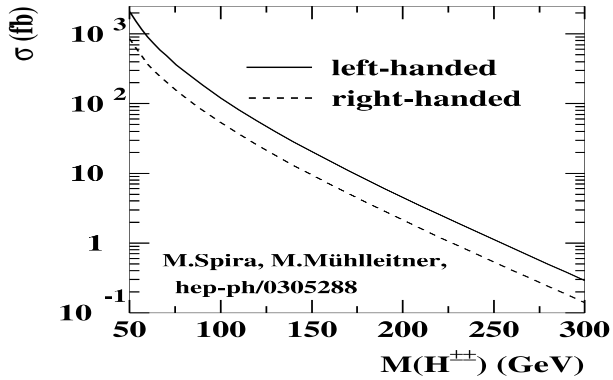

Figure 26: NLO cross section for $p\bar{p} \to H^{\pm\pm}$ production at the Tevatron, as a function of mass. [54]

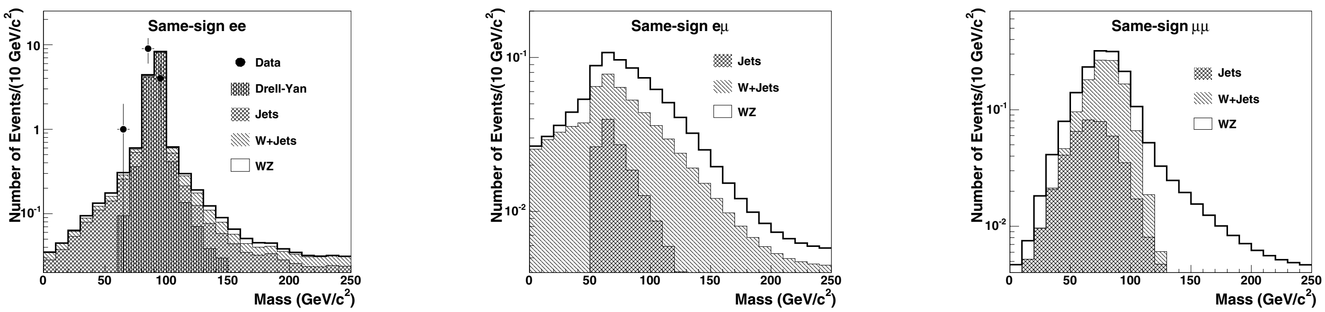

Figure 27: Same-sign dilepton mass distributions for the CDF doubly-charged Higgs boson search, along with the expectations from Standard Model backgrounds. [55]

mechanism at the Tevatron will be via Z/γ^*; see Figure 25. The cross section for the production process has been calculated at next-to-leading order [54] and is plotted in Figure 26. Note that the production cross section is different for left and right handed bosons.

Both experiments have searched for $H^{\pm\pm}$ decaying to dileptons. CDF's analysis [55] is based on about 240 pb^{-1} of data, and looks in the ee, $e\mu$, and $\mu\mu$ channels. CDF identifies electrons with $E_T > 30$ GeV and muons with $p_T > 25$ GeV/c and then selects events which have two same-sign leptons. They then plot the invariant masses of the lepton pairs; see Figure 27. The high-mass region with $m(\mu\mu), m(e\mu) > 80$ GeV/c^2 and $m(ee) > 100$ GeV/c^2 is used for the Higgs boson search. (The dielectron sample has a higher threshold to remove Z boson decays.) No events are observed in this region. The low-mass region defined by $m(\ell\ell) < 80$ GeV/c^2 is used to check the background predictions.

The backgrounds are listed in Table X and include:

- Multijet events where two jets are misidentified as leptons. The estimate for this is derived from data.
- W+jets events where one jet is misidentified as a lepton. The estimate for this is derived from data. Background from $W\gamma$ is studied with Monte Carlo and is found to be negligible.
- $Z/\gamma^* \to e^+e^-$ where one electron converts to a photon which subsequently radiates a e^+e^- pair. This background is studied using Monte Carlo, normalized using the background-subtracted number of same-sign candidates in the Z boson peak.
- Cosmic ray background is estimated using muon detector timing information.

Table X: The total estimated backgrounds for the CDF doubly-charged Higgs boson search for the low-mass ($< 80\,\mathrm{GeV}/c^2$) and high-mass (100–300 GeV/c^2 for ee, 80–300 GeV/c^2 for $\mu\mu$ and $e\mu$) regions. [55]

	ee		$\mu\mu$		$e\mu$	
Background	Low-Mass	High-Mass	Low-Mass	High-Mass	Low-Mass	High-Mass
$Z/\gamma^* \to \ell\ell$	0.46 ± 0.13	0.37 ± 0.11				
Jets$\to \ell\ell$	$0.47^{+0.23}_{-0.19}$	$0.62^{+0.71}_{-0.44}$	$0.30^{+0.24}_{-0.16}$	$0.19^{+0.35}_{-0.17}$	0.09 ± 0.05	0.06 ± 0.05
$W + \mathrm{jet} \to \ell\ell$	0.14 ± 0.08	0.36 ± 0.21	0.32 ± 0.22	0.40 ± 0.27	$0.22^{+0.24}_{-0.15}$	0.25 ± 0.17
$WZ \to \ell\ell$	0.07 ± 0.02	0.11 ± 0.03	0.21 ± 0.04	0.19 ± 0.03	0.12 ± 0.02	0.12 ± 0.03
Total Background	1.1 ± 0.4	$1.5^{+0.9}_{-0.6}$	0.8 ± 0.4	$0.8^{+0.5}_{-0.4}$	0.4 ± 0.2	0.4 ± 0.2
Observed	1	0	0	0	0	0

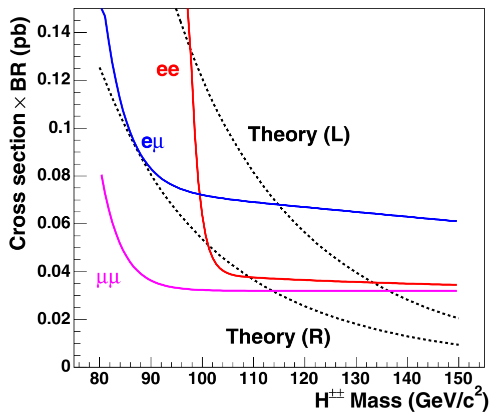

Figure 28: Experimental limits on cross section times branching ratio at 95% C.L. as a function of $H^{\pm\pm}$ mass (solid curves). The dotted curves show the next-to-leading order calculations [54]. For the CDF doubly-charged Higgs boson search. [55]

The acceptance for $H^{\pm\pm}$ decays is found from Monte Carlo. For the ee and $e\mu$ channels, it is $\approx 34\%$, and for the $\mu\mu$ channel, $\approx 18\%$. From this, the 95% C.L. limits can be extracted; see Figure 28. Then, from the next-to-leading order production cross sections and the assumption that $H^{\pm\pm}$ decays exclusively to the mode being considered, we have the following limits:

- $H^{\pm\pm} \to ee$: $m(H_L^{\pm\pm}) > 133\,\mathrm{GeV}/c^2$.
- $H^{\pm\pm} \to e\mu$: $m(H_L^{\pm\pm}) > 115\,\mathrm{GeV}/c^2$.
- $H^{\pm\pm} \to \mu\mu$: $m(H_L^{\pm\pm}) > 136\,\mathrm{GeV}/c^2$ and $m(H_R^{\pm\pm}) > 113\,\mathrm{GeV}/c^2$.

The DØ analysis is based on about $113\,\mathrm{pb}^{-1}$ of data, and uses only the dimuon channel [56]. Events are selected using the following requirements:

- S1. At least two muon candidates with $p_T > 15\,\mathrm{GeV}/c$.
- S2. There must be no large deposits in the calorimeter around the muon tracks. This rejects muons originating from b-decays.
- S3. $\Delta\phi(\mu\mu) < 0.8\pi$. This is only applied for events with exactly two muons. It rejects background due to $Z \to \mu\mu$ (where one charge is mismeasured) and from cosmic-ray muons.
- S4. At least one pair of muons with the same-sign charge.

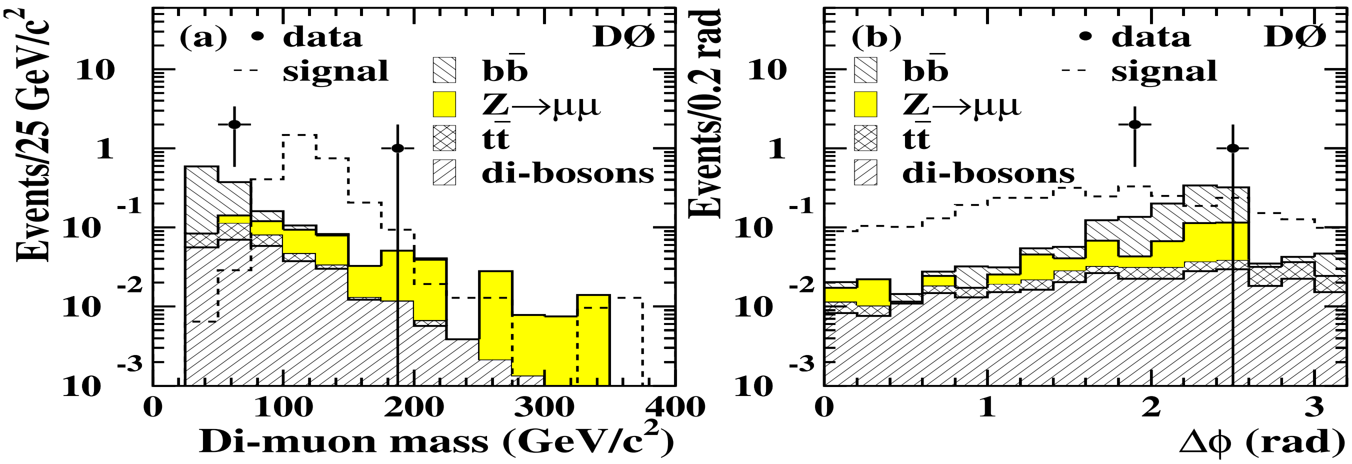

Figure 29: (a) Dimuon mass and (b) $\Delta\phi$ for the two like-charge muons of highest p_T. The data are compared to the expected Standard Model background. The signal histogram drawn is for $m(H_L^{\pm\pm}) = 120\,\mathrm{GeV}/c^2$. Note that the $\Delta\phi$ requirement is only applied to events with exactly two muons, so that events with three or more muons can have $\Delta\phi > 0.8\pi$. For the DØ doubly-charged Higgs boson search. [56]

Table XI: Number of data events, calculated background, and expected signal for $m(H_L^{\pm\pm}) = 100\,\mathrm{GeV}/c^2$ after each selection, for the DØ doubly-charged Higgs boson search. [56]

Selection	S1	S2	S3	S4
Signal	9.4	8.5	7.5	6.5
$Z\to\mu^+\mu^-$	4816	4055	359	0.3 ± 0.1
$b\bar{b}$	391	18	3.0	0.8 ± 0.4
$Z\to\tau^+\tau^-$	40	34	2.4	< 0.1
$t\bar{t}$	3.0	2.1	1.5	0.11 ± 0.01
ZZ	0.1	0.1	0.1	0.05 ± 0.01
WZ	0.6	0.5	0.4	0.23 ± 0.01
WW	3.5	3.1	1.9	< 0.01
Total background	5254 ± 47	4113 ± 43	368 ± 14	1.5 ± 0.4
Data	5168	4133	378	3

Plots of the events passing these requirements are shown in Figure 29. A summary of the number of events passing each of the requirements and the expected Standard Model background is given in Table XI.

The total acceptance for $H^{\pm\pm}$ is evaluated as a function of Higgs boson mass, and is found to be about 50%. Thus, a limit is extracted; see Figure 30. Assuming that the $H^{\pm\pm}$ decays entirely to $\mu\mu$, we get $m(H_L^{\pm\pm}) > 118.4\,\mathrm{GeV}/c^2$ and $m(H_R^{\pm\pm}) > 98.2\,\mathrm{GeV}/c^2$.

5. Long-term Higgs boson sensitivity

In 2004, the Fermilab Tevatron performed very well, accumulating nearly $350\,\mathrm{pb}^{-1}$ of data. This exceeded the optimistic goals that had been set for the year. Several major improvements to the complex are still planned for the next several years [57]. Following the completion of the fall 2004 shutdown, the Main Injector is expected to run in "slip-stacking" mode, in which multiple proton bunches from the Booster are merged into single bunches in the Main Injector. This allows a larger beam current in the Main Injector and hence a higher rate of antiproton production. Towards the end of 2005, it is anticipated to start using electron cooling in the Recycler. In this

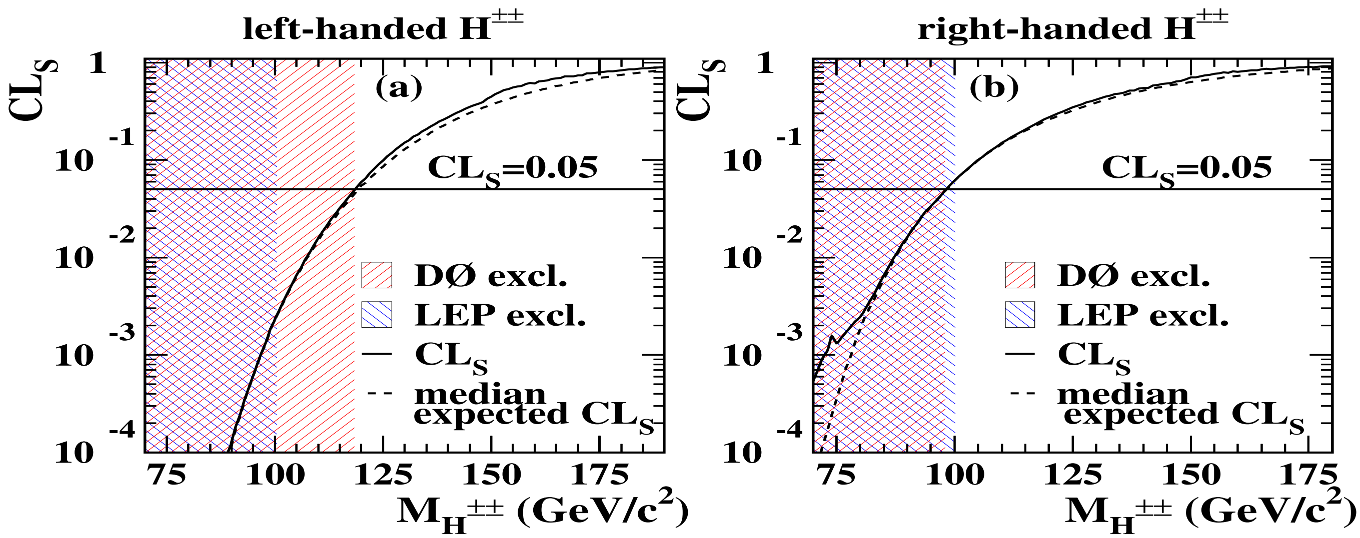

Figure 30: Confidence level of the signal $\mathrm{CL}_S = \mathrm{CL}_{S+B}/\mathrm{CL}_B$, as a function of Higgs boson mass, for both left-handed and right-handed Higgs bosons. Masses with $\mathrm{CL}_S < 0.05$ are excluded by this analysis. The region below about $100\,\mathrm{GeV}/c^2$ is excluded by LEP. The dashed curve shows what the result would have been had no candidates been observed. For the DØ doubly-charged Higgs boson search. [56]

technique, an electron beam traveling parallel to the antiproton beam can cool the antiprotons more effectively than the conventional stochastic cooling. Other upgrades to the antiproton source and the Tevatron are also planned.

For planning purposes, two projections of integrated luminosity are given through the end of 2009. The "design" (challenging) projection assumes that every planned improvement is ready on time and works at least as well as anticipated. This projection is for about $8\,\mathrm{fb}^{-1}$ by the end of 2009 (this projection as of September, 2004 [58]). The "base" (conservative) projection makes allowances for schedule slippage and underperformance; this projection is for about $4\,\mathrm{fb}^{-1}$ by 2009.

In 2003, a working group was formed to revisit the question of what is the long-term Higgs boson mass reach of the Tevatron experiments, as a function of the total integrated luminosity. The results are reported in [5] and summarized in Figure 31. For the base projection of $4\,\mathrm{fb}^{-1}$, one would expect to be able to exclude masses up to $\sim 130\,\mathrm{GeV}/c^2$ and to have a 3σ signal for masses up to $\sim$ 120–125 GeV/c^2. For the design projection of $8\,\mathrm{fb}^{-1}$, one would expect to have a 3σ signal for masses up to $\sim 130\,\mathrm{GeV}/c^2$ and a 5σ discovery for masses up to $\sim$ 115–120 GeV/c^2. (One caveat: the study assumed that the vertex detectors of the two experiments would be upgraded as originally planned. These upgrades have now been canceled, but the effects of this on the Higgs boson sensitivity have not been systematically evaluated.)

6. Summary and conclusions

In 2004, many results relevant to the Higgs boson search have started to emerge from the Tevatron experiments. Most of the results reported here have been based on data samples of 100–200 pb^{-1}, which is only about half of what has been recorded so far. The Higgs boson analyses to date have been mainly focused on understanding the performance of the detectors and the various background processes. However, the Tevatron can already set competitive limits for some non-Standard Model processes. The Tevatron has performed better than expected over the last year, and data will continue to accumulate for many years to come.

In conclusion, the Standard Model Higgs boson is very challenging to find. But if the performance projections hold up, the Tevatron will have sensitivity to an interesting range of Higgs boson masses.

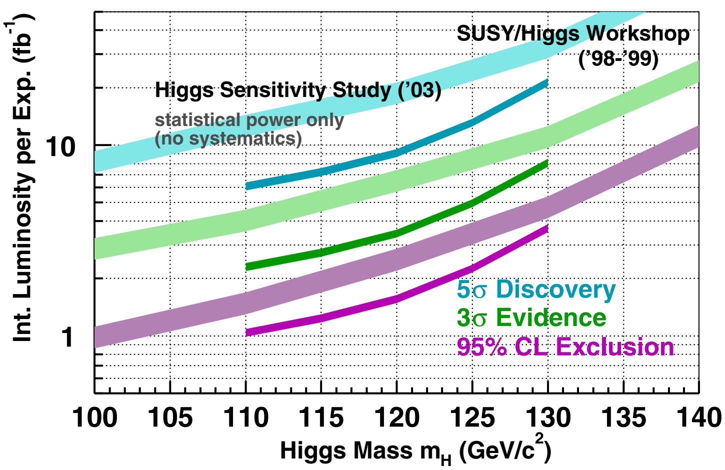

Figure 31: Integrated luminosities per experiment corresponding to the median expectations for 95% C.L. exclusion, 3σ evidence, and 5σ discovery as a function of m_H. The narrow curves are from the newer study of [5]; the thicker curves are from a previous study [3].

Acknowledgments

Sincere thanks go to the staff of the Fermilab Beams Division as well as the members of the CDF and DØ collaborations for the rich selection of results on which to report. This work is supported in part by the U.S. Department of Energy under contract DE-AC02-98CH10886 with Brookhaven National Laboratory.

References

[1] R. Barate et al. (The LEP Working Group for Higgs Boson Searches), Phys. Lett. **B565**, 61 (2003), hep-ex/0306033.

[2] The LEP Electroweak Working Group, URL `http://lepewwg.web.cern.ch/LEPEWWG/`.

[3] M. Carena et al. (Higgs Working Group) (2000), hep-ph/0010338.

[4] *The Higgs working group: Summary report*, FERMILAB-CONF-01-477 (2002), hep-ph/0203056.

[5] L. Babukhadia et al. (CDF and D0 Working Group Members) (2003), FERMILAB-PUB-03-320-E, URL `http://library.fnal.gov/archive/2003/pub/fermilab-pub-03-320-e.pdf`.

[6] J. F. Gunion, H. E. Haber, G. Kane, and S. Dawson, *The Higgs Hunter's Guide* (Addison-Wesley, New York, 1990).

[7] M. Spira (1998), contributed to Physics at Run II: Workshop on Supersymmetry / Higgs: Summary Meeting, Batavia, IL, 19-21 Nov 1998, hep-ph/9810289.

[8] A. Djouadi, J. Kalinowski, and M. Spira, Comput. Phys. Commun. **108**, 56 (1998), hep-ph/9704448.

[9] URL `http://www-cdf.fnal.gov/`.

[10] URL `http://www-d0.fnal.gov/`.

[11] V. M. Abazov (D0) (2004), submitted to Phys. Rev. Lett., hep-ex/0410062.

[12] CDF collaboration (2004), CDF/PUB/EXOTIC/PUBLIC/7126, URL `http://www-cdf.fnal.gov/physics/exotic/old.pub_notes/cdf7126_WX_Searches.pdf`.

[13] V. M. Abazov (D0) (2004), submitted to Phys. Rev. Lett., hep-ex/0410078.

[14] J. Campbell, R. K. Ellis, F. Maltoni, and S. Willenbrock, Phys. Rev. **D69**, 074021 (2004), hep-ph/0312024.

[15] DØ collaboration (2004), DØNote 4387-CONF, URL `http://www-d0.fnal.gov/Run2Physics/WWW/results/prelim/HIGGS/H03/H03.pdf`.

[16] E. Arik et al., Eur. Phys. J. **C26**, 9 (2002), hep-ph/0109037.
[17] CDF collaboration (2004), CDF/PUB/EXOTIC/PUBLIC/7152, URL `http://www-cdf.fnal.gov/physics/exotic/old.pub_notes/cdf7152_hwwlvlv_pub_2.pdf`.
[18] S. Mrenna and J. D. Wells, Phys. Rev. **D63**, 015006 (2001), hep-ph/0001226.
[19] H. E. Haber, G. L. Kane, and T. Sterling, Nucl. Phys. **B161**, 493 (1979).
[20] J. F. Gunion, R. Vega, and J. Wudka, Phys. Rev. **D42**, 1673 (1990).
[21] B. Grzadkowski and J. F. Gunion, Phys. Lett. **B473**, 50 (2000), hep-ph/9910456.
[22] B. A. Dobrescu, Phys. Rev. **D63**, 015004 (2001), hep-ph/9908391.
[23] B. A. Dobrescu, G. Landsberg, and K. T. Matchev, Phys. Rev. **D63**, 075003 (2001), hep-ph/0005308.
[24] J. D. Wells, Phys. Rev. **D56**, 1504 (1997), hep-ph/9612292.
[25] H. Baer and J. D. Wells, Phys. Rev. **D57**, 4446 (1998), hep-ph/9710368.
[26] L. J. Hall and C. F. Kolda, Phys. Lett. **B459**, 213 (1999), hep-ph/9904236.
[27] H.-C. Cheng, B. A. Dobrescu, and C. T. Hill, Nucl. Phys. **B589**, 249 (2000), hep-ph/9912343.
[28] DØ collaboration (2004), DØNote 4374-CONF, URL `http://www-d0.fnal.gov/Run2Physics/higgs/docs/Spring_2004/dilepton/h_d0conf_APPROVED.pdf`.
[29] G. Landsberg and K. T. Matchev, Phys. Rev. **D62**, 035004 (2000), hep-ex/0001007.
[30] B. Abbott et al. (DØ), Phys. Rev. Lett. **82**, 2244 (1999), hep-ex/9811029.
[31] A. Rosca (LEP), in *Amsterdam 2002, ICHEP* (2002), pp. 743–745, hep-ex/0212038.
[32] A. G. Akeroyd, Phys. Lett. **B368**, 89 (1996), hep-ph/9511347.
[33] LEP Higgs Working Group (2001), hep-ex/0107030.
[34] T. Affolder et al. (CDF), Phys. Rev. Lett. **86**, 4472 (2001), hep-ex/0010052.
[35] DØ collaboration (2004), DØNote 4366-CONF, URL `http://www-d0.fnal.gov/Run2Physics/higgs/docs/Spring_2004/bbh2004_files/notes/bbh_analysis_conf_v1.32.pdf`.
[36] J. Campbell, R. K. Ellis, F. Maltoni, and S. Willenbrock, Phys. Rev. **D67**, 095002 (2003), hep-ph/0204093.
[37] J. F. Gunion, C. Loomis, and K. T. Pitts, ECONF **C960625**, LTH096 (1996), hep-ph/9610237.
[38] T. P. Cheng and L.-F. Li, Phys. Rev. **D22**, 2860 (1980).
[39] R. N. Mohapatra and J. C. Pati, Phys. Rev. **D11**, 566 (1975).
[40] G. Senjanovic and R. N. Mohapatra, Phys. Rev. **D12**, 1502 (1975).
[41] R. N. Mohapatra and G. Senjanovic, Phys. Rev. **D23**, 165 (1981).
[42] C. S. Aulakh, A. Melfo, and G. Senjanovic, Phys. Rev. **D57**, 4174 (1998), hep-ph/9707256.
[43] Z. Chacko and R. N. Mohapatra, Phys. Rev. **D58**, 015003 (1998), hep-ph/9712359.
[44] T. G. Rizzo, Phys. Rev. **D25**, 1355 (1982), and Addendum ibid **27**, 657 (1983).
[45] H. Georgi and M. Machacek, Nucl. Phys. **B262**, 463 (1985).
[46] N. Arkani-Hamed, A. G. Cohen, E. Katz, and A. E. Nelson, JHEP **07**, 034 (2002), hep-ph/0206021.
[47] G. Abbiendi et al. (OPAL), Phys. Lett. **B577**, 93 (2003), hep-ex/0308052.
[48] R. N. Mohapatra, Phys. Rev. **D46**, 2990 (1992).
[49] G. W. Bennett et al. (Muon g-2), Phys. Rev. Lett. **92**, 161802 (2004), hep-ex/0401008.
[50] J. Abdallah et al. (DELPHI), Phys. Lett. **B552**, 127 (2003), hep-ex/0303026.
[51] G. Abbiendi et al. (OPAL), Phys. Lett. **B526**, 221 (2002), hep-ex/0111059.
[52] P. Achard et al. (L3), Phys. Lett. **B576**, 18 (2003), hep-ex/0309076.
[53] J. F. Gunion, J. Grifols, A. Mendez, B. Kayser, and F. I. Olness, Phys. Rev. **D40**, 1546 (1989).
[54] M. Muhlleitner and M. Spira, Phys. Rev. **D68**, 117701 (2003), and private communications, hep-ph/0305288.
[55] D. Acosta et al. (CDF) (2004), submittd to Phys. Rev. Lett., hep-ex/0406073.
[56] V. M. Abazov et al. (D0), Phys. Rev. Lett. **93**, 141801 (2004), hep-ex/0404015.
[57] For reports on the current status of the Tevatron upgrade project, see the Program Management Group page, URL `http://www.fnal.gov/directorate/runII_accel_pmg.html`.
[58] J. Spalding (2004), talk at DOE mini-review, URL `http://www-bdnew.fnal.gov/doereview04/mini/mini04_spalding2.pdf`.